Enhanced microlithography using coherent multiple imaging

Miklós Erdélyi, Károly Osvay, Zsolt Bor, William L. Wilson*, Michael C. Smayling*, and Frank K. Tittel*

JATE University, Department of Optics and Quantum Electronics, H-6720 Szeged, Dóm tér 9, P. O. Box 406, Hungary

*Rice University, Department of Electrical and Computer Engineering, 6100 Main Street, Houston TX 77251

ABSTRACT

An experimental and theoretical study of a coherent multiple imaging technique (CMI) that utilizes a Fabry-Perot etalon placed between the photo mask and the projection lens is reported. This technique can enhance both resolution and depth of focus in optical microlithography. A lithography simulation tool, Prolith/2, was used to evaluate the aerial image profile using a complex phase-amplitude pupil-plane filter to simulate the effect of the Fabry-Perot etalon. This work specifically discusses the evaluation of extended periodic patterns (line/space patterns and contact hole arrays), widely used in lithographic simulations. Simulation results are described and compared with experimental data. The impact of Talbot images generated by periodic structures is also described.

Keywords: Multiple imaging, Pupil-plane filtering, Microlithography, Resolution enhancement

1. INTRODUCTION

Coherent multiple imaging (*CMI*) is a potentially effective method to enhance both the minimum critical feature size and depth of focus in optical microlithography, suitable for KrF and ArF excimer laser illumination at wavelengths of 248 and 193 nm, respectively. While a conventional projection process creates a single image of the photo mask, *CMI* produces several images shifted along the optical axis. A *CMI* technique that uses a Fabry-Perot etalon placed between the mask and the projection lens was recently demonstrated by the authors both theoretically [1] and experimentally [2-3]. Such an etalon generates multiple images of the mask that are separated by 2d on the optical axis, where d is the separation of the etalon mirrors. The image produced by the projection lens is the superposition of the aerial images of the individual shifted images. The separation of the images behind the lens is $2dM^2$ where M^2 is the longitudinal magnification of the lens. It was demonstrated that an optimized etalon could enhance the depth of focus (*DOF*) and the resolution (*W*) of a single on-axis contact hole by 300% and 60%, respectively. However, simulation of extended mask patterns was not possible due to the limitations of the wave optics model that was used in this previous work.

A simple and fast simulation process is possible using an appropriate pupil-plane filter. It has been shown that a phase-amplitude filter could represent the effect of a Fabry-Perot etalon placed between the mask and the projection lens [4-5]. The simulation process is fast since it requires only one simulation run instead of multiple ones. Furthermore, a pupil plane filter can be defined in any simulation tool and the simulation does not require any software modification, which would be the case for a direct, multiple image approach.

In this paper, simulation data of extended periodical patterns based on optical lithography simulator Prolith/2 will be studied and compared to the experimental results. Detailed studies of Talbot images (which occur when extended periodical patterns are imaged), focus shift (introduced by the special phase property of the filter), light loss and generation of high intensity side lobes (introduced by the amplitude

Part of the EUROPTO Conference on Lithography for Semiconductor Manufacturing
Edinburgh, Scotland • May 1999
SPIE Vol. 3741 • 0277-786X/99/$10.00

property of the filter) will be discussed. This paper also suggests methods to address and minimize the effects mentioned above.

2. IMAGING OF EXTENDED PERIODICAL PATTERNS — TALBOT IMAGES

An extended periodic structure (line-space patterns, contact hole arrays *etc.*) illuminated by a normally incident plane wave, will form periodic images of the original mask pattern. This effect was first observed by Talbot in 1836 [6], and theoretically described by Rayleigh in 1881 [7]. He showed that the Talbot distance (d_T) between the images is

$$d_T = 2\Lambda^2/\lambda, \qquad (1)$$

where Λ is the period on the mask, and λ is the wavelength. Between the Talbot images, phase reversed images and subimages appear, respectively. Figure 1 shows a simplified model of the generation of Talbot images. Talbot images are not the results of a traditional imaging process. The rays that form a specific pattern in the Talbot plane, are not generated by one mask pattern, but by different patterns. However, assuming a periodic and infinite mask structure, the Talbot images will be perfect replicas of the mask.

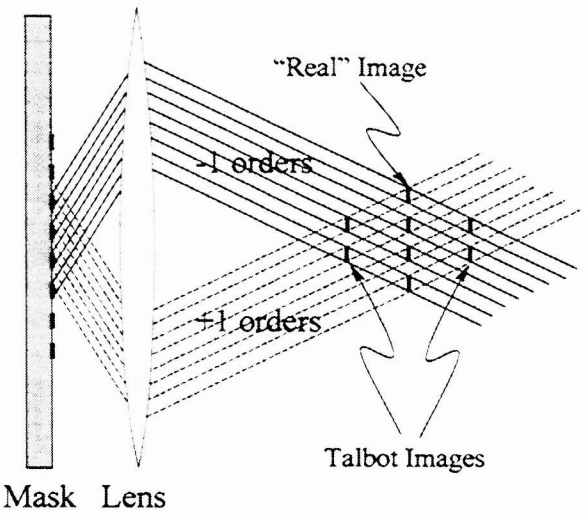

Figure 1. Simplified geometrical explanation for generation of Talbot images. Talbot images are not the result of a traditional imaging process. The rays that form a specific pattern in the Talbot plane are generated by different patterns.

Since in state-of-the art optical microlithography pitches are typically in the range of several wavelengths, the appropriate Talbot distances could be equal to or even smaller than the *DOF*. Direct (the images overlap, because d_T<*DOF*) and indirect (the images overlap due to multiple reflection) interference between the images can reduce the image quality within the resist film. On the other hand, real patterns are

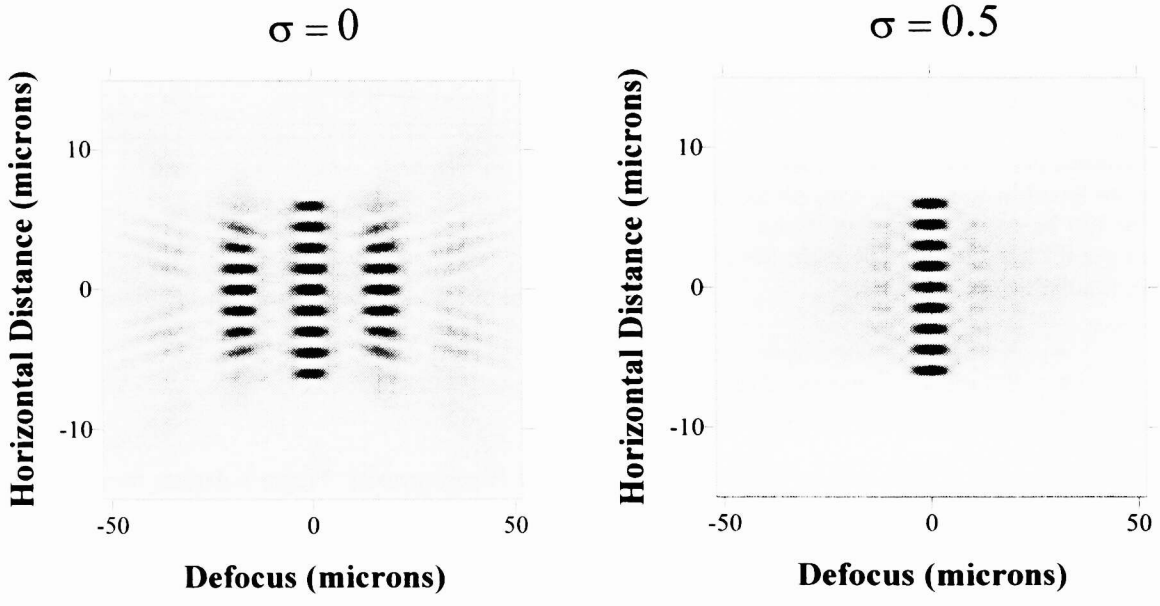

Figure 2. The impact of spatial coherence on the Talbot images. The Talbot images disappear when using partially coherent illumination.

not infinitely large. The Talbot images of a finite extent periodic structure are not exact replicas of the original mask. At the edge of the structure – where the diffraction orders do not overlap – the visibility decreases rapidly, and not all patterns are "imaged". Talbot images can lead to serious image quality degradation.

Since Talbot images are generated by the action of all features across the mask, they can be eliminated by decreasing the spatial coherence (σ) of the illumination. Using partially coherent illumination, the diffracted rays depicted in Figure 1 are not coherent, and they cannot create an image. Figure 2 shows the cross section of the aerial images of a contact hole array at various distances from the lens. The cross section contains 9 holes (CD=0.5μm) with 1.5 micron separation. The illumination wavelength was chosen to be 248nm. Using coherent illumination (σ=0) the Talbot images (18 microns in front and behind the real image) can be seen clearly. Due to the finite extent of the mask, the image is created in the central part only, where the ±1 diffraction orders overlap. The higher diffraction orders do not contribute to the image since they are out of the aperture of the lens. These images are not exact replicas of the mask, however, the edges of the structure are not imaged, and only the three holes in the middle of the structure can be observed. However, when the spatial coherence is decreased (σ=0.5), the images disappear.

3. CMI BY MEANS OF PUPIL PLANE FILTERING

A Fabry-Perot interferometer placed between the mask and the projection lens can be considered as a spatial filter that transmits certain spatial Fourier components of the mask pattern while blocking others. Using this analogy, the etalon can be perfectly simulated by a pupil-plane filter.

Enhanced image formation by means of modified pupil filtering has been previously investigated by several authors. For example, the super-FLEX method reported by Fukuda et. al. [8], introduces a pupil plane filter that shifts the focal plane by $\pm\beta$, and the phase by $\pm\Delta\varphi$, respectively. The total electric field is the superposition of these two images. In the Fabry-Perot approach the images behind the projection lens are shifted by $2dM^2$, $4dM^2$, $6dM^2$..., while the phase is shifted by φ, 2φ, 3φ..., and the amplitude ratio between the adjacent images is R (the reflectivity of the mirrors). The total electric field is the superposition of these fields. A detailed theoretical description of such pupil-plane filters can be found in Ref. [4-5]. This phase-amplitude filter can be easily defined in Prolith/2 using a lens pupil filter file [9]. The main advantages of this simulation approach are:

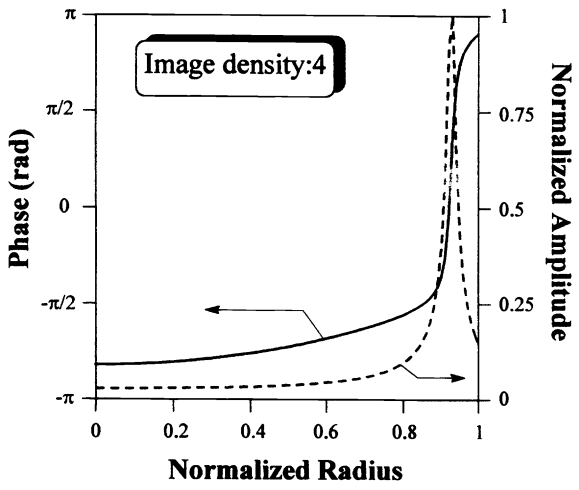

Figure 3. Normalized amplitude and phase distribution of the pupil plane filter. The relative image density is 4.

- A single run simulation is required instead of multiple runs.
- Simulation of extended mask structures becomes feasible.
- No software modifications are required.

In this paper such a filter will be studied theoretically and experimentally. Figure 3 depicts the amplitude and phase properties of the filter. The input stepper parameters used to run Prolith simulation are the following:

- Image Calculation Mode: Full Scalar
- Numerical Aperture: 0.3
- Wavelength: 441.6 nm (CW HeCd laser)
- Reduction (1/M): 5

- Spatial Coherence (σ): 0

The depth of focus and resolution limit of this system using the Rayleigh equations (DOF=2λ/NA^2, CD=0.61λ/NA) are 9.8 and 0.9 μm, respectively.

The pupil plane filter depicted in Figure 3 substitutes for a Fabry-Perot interferometer with a mirror separation of d=122 μm and mirror reflectivity of R=0.97. The relative image density (defined by the number of images in one *DOF* range: $N=DOF/2dM^2$) behind the projection lens is 4. The filter is optimized so that the amplitude transmission maximum is very close to the edge of the aperture (the relative position of the main peak is 0.92). The phase changes very rapidly where the filter transmits the incident light. This special phase property of the filter introduces a shift of the main intensity peak along the optical axis, as will be discussed below. Since the reflectivity of the mirrors is high, and the relative image density is relatively small, the transmission ring of the filter is narrow. In the next sections, where extended periodical structures will be evaluated theoretically and experimentally, the light loss introduced by the spatially narrow bandwidth filter will also be discussed.

4. IMAGING OF LINE-SPACE PATTERNS

In this section, 9 line-space patterns with different pitches, but with the same pitch/CD are evaluated theoretically and experimentally. The pitch is changed in the range of 2 to 1.36 μm in steps of 0.08 μm. The pitch/CD is 2, so that the width of the lines is equal to their separations. Every pattern contains ten lines with a length of 10 μm.

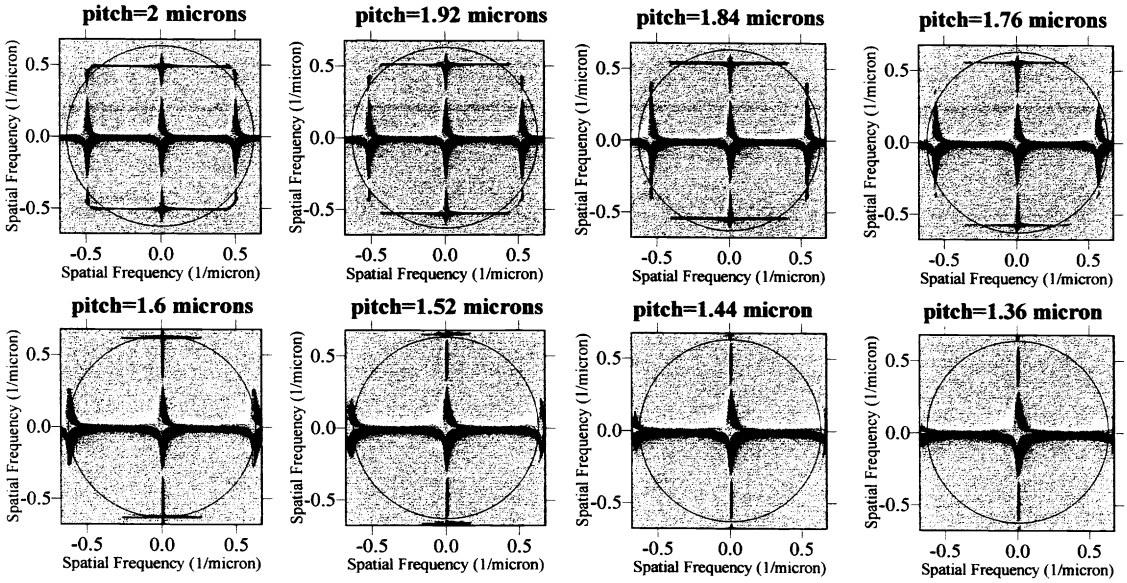

Figure 4. 2D intensity distribution in the Fourier plane using line-space patterns with different pitches. The pattern can be imaged if the first diffraction orders are inside the aperture (resolution limit for pitch ~1.47 μm).

A HeCd laser operating at 441.6 nm illuminated the mask pattern. The beam intensity was controlled by two polarizers. A scanning Fabry-Perot interferometer (d=122 μm, R=0.97) was placed between the mask and the projection lens to generate the multiple images of the mask. The projection lens was a g-line (436 nm) stepper lens manufactured by Tropel Inc. with numerical aperture of NA=0.3 and reduction of M=5. The image produced by the projection lens was magnified by two microscope objective in tandem (with about 800X overall magnification) and monitored with a charge coupled device (CCD) camera.

Figure 4 depicts the 2D Fourier transforms (the 2D intensity distribution in the pupil-plane) of eight patterns. The maximum spatial frequency transmitted by the lens is determined by the numerical aperture of the lens and the illumination wavelength ($v_{max}=NA/\lambda=0.68$ *1/μm*). If we decrease the pitch, the diffraction angle of the ±1 orders increases. A line-space pattern can be imaged (using a conventional

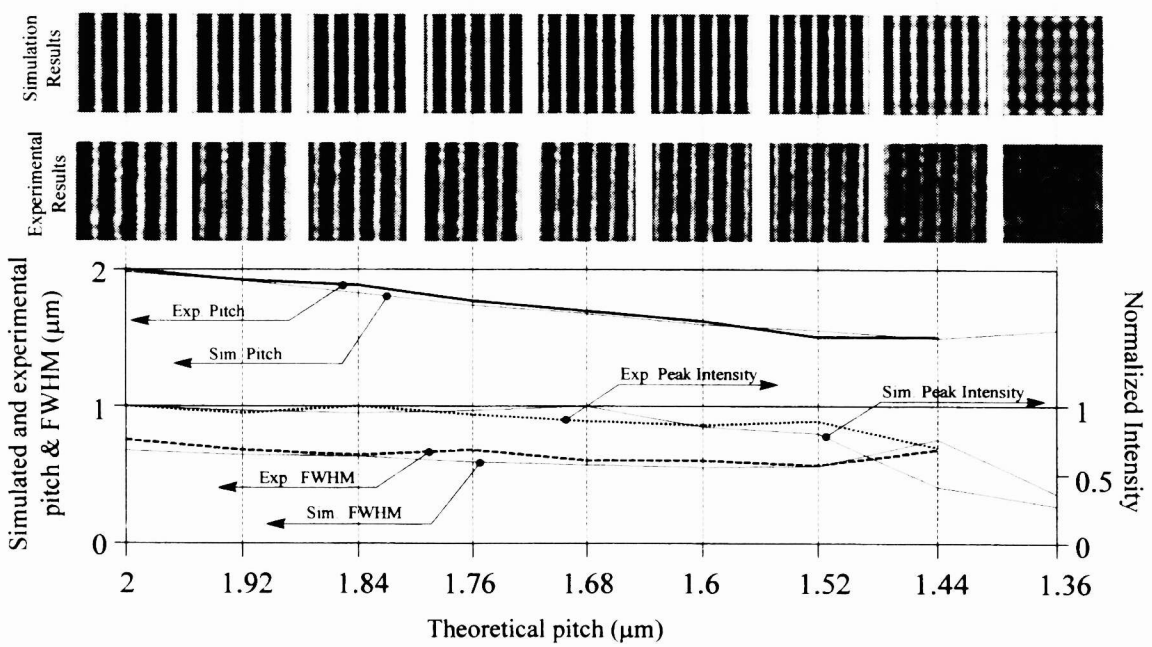

Figure 5. Simulation and experimental results in focus (defocus=0) without filter. The size of the windows are 9 by 9 microns.

projection system), if at least three diffraction orders contribute to the final image. Since the position of the zero order does not change (it is on the optical axis, therefore it is always transmitted by the lens), the resolution depends on the position of the ±1 diffraction orders. However, the diffraction angle depends only on the wavelength/pitch ratio, and is independent of the width of the lines. According to Figure 4, the line-space pattern with 1.52 μm pitch can still be resolved, while the 1.44 μm pattern is below the resolution limit of the lens. Using simple geometrical optics considerations, the resolution limit (*resolvable pitch= λ/NA*) is 1.47 μm, which is in good agreement with the result of the Fourier optics model. Figure 4 also shows the position of the amplitude maximum of the filter (circles with a radius of 0.68*0.92=0.62 1/μm).

Figure 5 shows the aerial images of the nine line-space patterns in the optimum focal plane (defocus=0) without a filter. The simulation results (upper row) agree with the experimental results (lower row). The pattern with 1.52 μm pitch is the smallest resolvable pattern. The *FWHM* values and the pitches were calibrated using the largest pattern. Above the resolution limit both the pitches and the *FWHM* values follow the theoretical values. The gradient of the *FWHM* curve is half of the pitch curve. The normalized intensity curves show that the peak intensities do not change significantly above the resolution limit. However, using patterns with smaller pitch than the resolution, the *FWHM* of the lines starts to increase, and the peak intensity decreases rapidly.

The aerial images generated with the pupil-plane filter discussed in Section 3 can be seen in Figure 6. The filter shifts the intensity maximum on the optical axis by 5 μm towards the lens. Therefore, both simulation and experimental data depicted in Figure 6 were obtained by introducing a –5 μm defocus. The presence of the pupil-plane filter changes the aerial image significantly. The zero diffraction order is always blocked, so that the angle between the diffraction orders that generate the final image doubles. Due to this fact, the period of the generated pattern is also doubled. It is important to note that the doubled periodicity is caused by the missing zero order, and not by an interference effect between the "real" lines.

Due to the narrow bandwidth of the filter, the system is very pitch sensitive. A line-space pattern can be projected if its first diffraction orders can be transmitted by the filter. This is the reason why Filter 6 shows only 3 patterns. The filter essentially blocks all the diffraction orders of the other patterns. In the case of 1.6 μm pitch, the amplitude maximum of the filter crosses the first diffraction orders of the pattern. This is an optimum case, as far as light loss is concerned. The peak intensities of the adjacent patterns (with 1.68 and 1.52 μm pitches) decrease rapidly. The *FWHM* of the lines is decreased by 25% (from 0.56 μm to 0.42 μm).

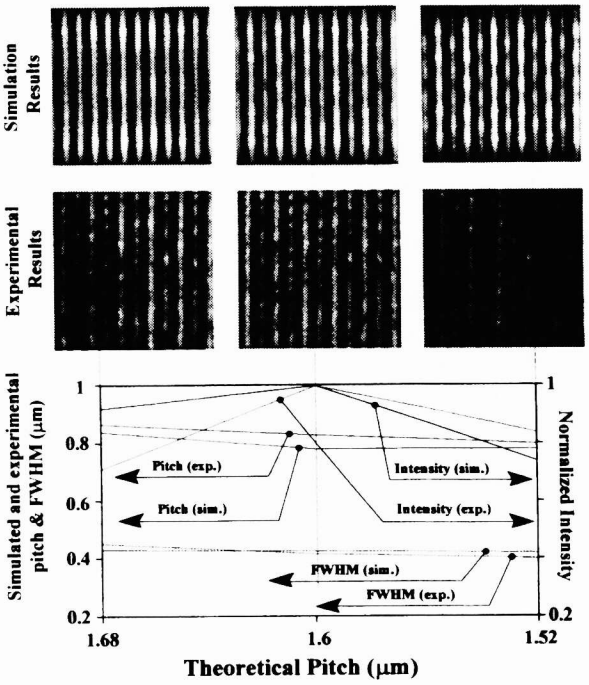

Figure 6. Simulation and experimental results with a filter. Defocus=-5 μm.

The aerial image of the optimum line-space pattern (1.6 μm pitch) was also evaluated using different defocus values. The first and the second rows in Figure 7 depict the simulation and experimental results without a filter, respectively. Since the intensity distribution is symmetrical with respect to the focal point, Figure 7 shows only the defocus range from −3 to 0 μm. The *DOF* is ~4 μm. The filter significantly increases the *DOF* value. The third and the fourth rows depict the simulation and experimental results with a filter, respectively. It can be

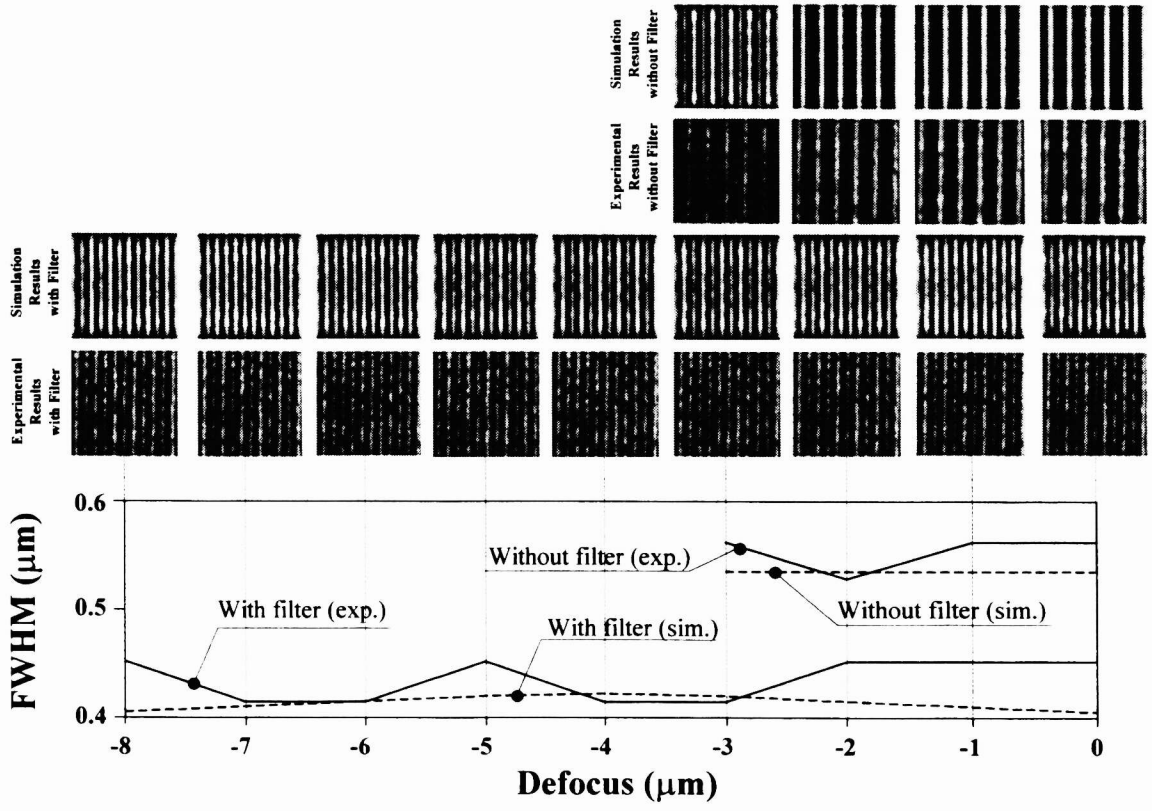

Figure 7. Simulation and experimental results in the presence and in the absence of the filter using line-space pattern with 1.6 μm pitch. The filter significantly increases the depth of focus and enhances the resolution.

seen that the *DOF* of the doubled periodicity pattern is increased significantly. As seen from the experimental results, the filter increased the *DOF* by 27/3=9X, while maintaining the 25% enhancement in *FWHM*.

The filter with a narrow bandwidth introduces not only a pitch sensitivity into the system, but also light loss. Since the bandwidth of the filter is narrower than the width of the first diffraction order, the filter transmits only a part of the first diffraction order. The Fabry-Perot ring and the diffraction orders (zero and first orders) can be seen in Figure 8. The figure represents an optimum case, when the Fabry-Perot ring is in the middle of the first order. The simulation and experimental results show that the peak intensity decreases to ~4% of the original maximum when using the filter. This significant light loss can be avoided by means of a Fabry-Perot etalon that has lower reflectivity mirrors. In an optimum case, the bandwidth of the filter is equal to the width of the first diffraction order, so that the filter transmits the ±1 diffraction orders, and the peak intensity will reach 30% of the original maximum.

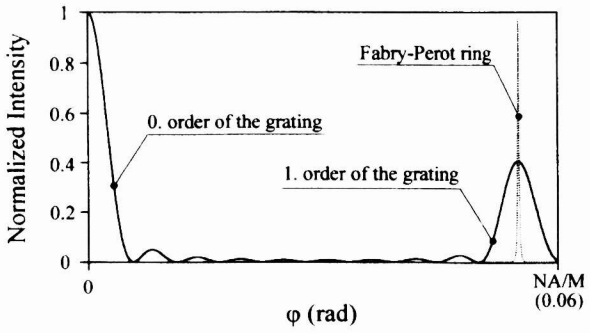

Figure 8. Normalized intensity distribution of the diffraction orders of the grating and the Fabry-Perot ring inside the aperture. In an optimum case, the maxima of the Fabry-Perot ring and the first diffraction order overlap.

5. IMAGING OF CONTACT HOLE ARRAYS

Besides the line-space patterns, 13 off-set contact hole arrays — with different hole sizes (in the range of 1 to 0.52 μm in steps of 0.04 μm) but with the same hole pitch/hole size ratio of 6 — were also investigated.

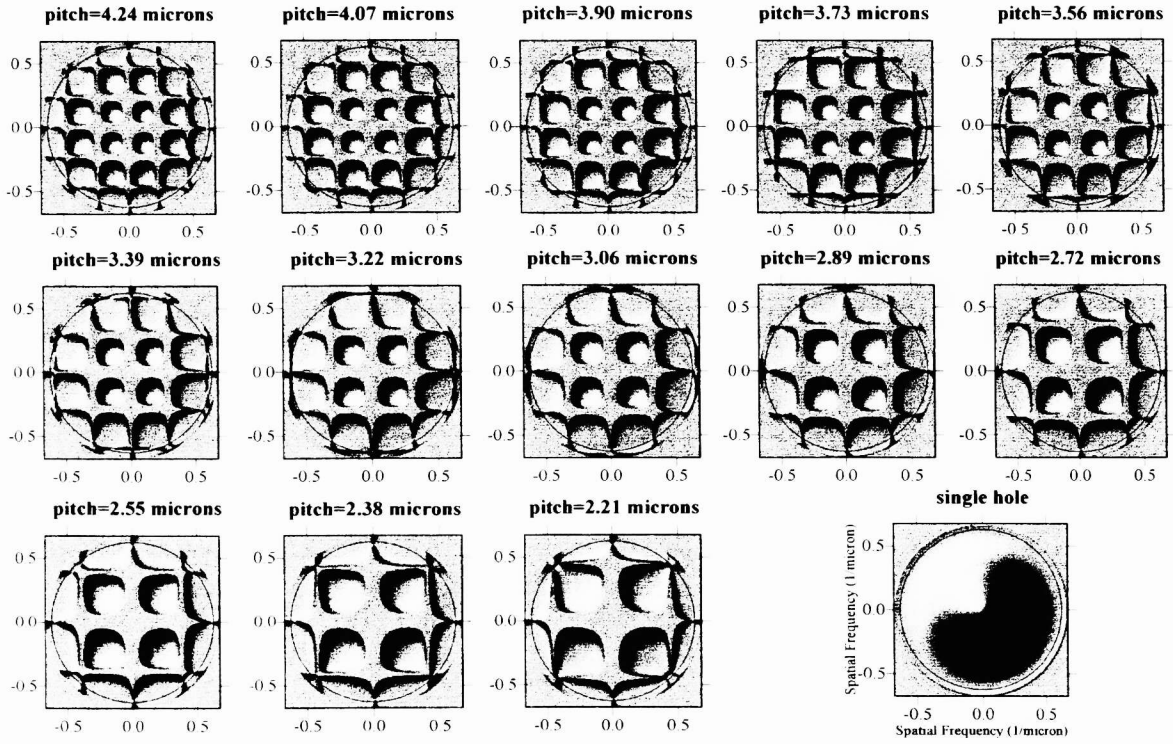

Figure 9. 2D intensity distribution in the Fourier plane using contact hole arrays with different pitches.

Figure 9 shows the 2D intensity distribution in the Fourier plane of the projection lens using contact hole arrays with different pitches . The position of the amplitude maximum of the filter is depicted by a circle with a radius of 0.62.

The spatial Fourier transform of a hole array is complex, since this is a 2D problem. As a reference, Figure 9 also depicts the intensity distribution in the pupil-plane using a single on-axis hole. The filter introduces a strong pitch sensitivity into the system. In an optimum case (when the pitch is 3.56 μm), the filter decreases the *FWHM* of the holes by 29% and the *DOF* by 300% . However, the peak intensity is ~4% of the original maximum. The light loss can be improved in the same manner as in the previous section.

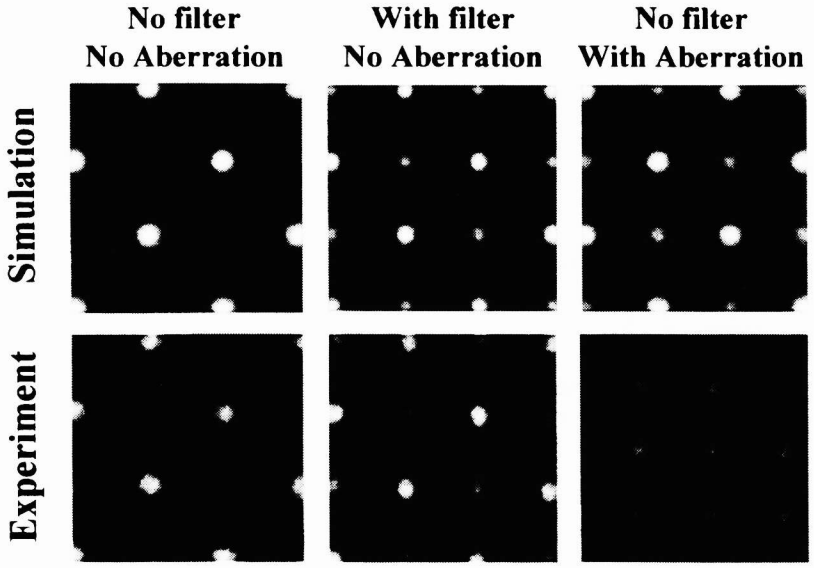

Figure 10. Simulation and experimental results using an off-set contact hole array. In the presence of both the filter and optical aberration the side lobes increase and produce high intensity secondary maxima.

Figure 10 depicts the experimental and simulation results using the optimum pattern. The aerial images without filter and without serious optical aberrations are essentially perfect replicas of the photo mask. There are no undesirable secondary intensity maxima between the real holes. However, introducing a filter or optical aberration into the system, the profile of the aerial image changes significantly. Interference between the increased intensity side lobes generates high intensity secondary maxima. These maxima have sometimes higher intensity than the original hole images themselves. Two methods were proposed by the authors recently [5] to decrease the intensity of the secondary interference maxima. The first method changes the spatial coherence of the illumination. The optimum value of spatial coherence was found to be 0.28. The other method introduced a π phase shift between the adjacent holes. Due to the destructive interference between the opposite fields, the secondary maxima disappears.

6. CONCLUSION

It was demonstrated that an optimized Fabry-Perot etalon placed between the mask and the projection lens is able to enhance the aerial image of extended periodical patterns (such as line-space patterns and contact hole arrays). The etalon was simulated by means of a complex phase-amplitude pupil plane filter using Prolith/2.

A detailed comparative study of simulation and experimental results showed that the etalon increases the resolution by 25-29% and the DOF by 300%-900% depending on what pattern is selected. The pitch sensitivity and the light loss introduced by the narrow bandwidth filter were also discussed. Two methods were proposed to decrease the intensity of the secondary maxima caused by the constructive interference between the diffraction rings.

ACKNOWLEDGEMENT

This research was supported in part by the Texas Instruments Inc. University Research program and by the OTKA Foundation of the Hungarian Academy of Sciences (T020910). We would like to thank FINLE Technologies for providing its support by making Prolith/2 available to this study.

REFERENCES

1. Z. L. Horvath, M. Erdelyi, G. Szabo, Zs. Bor, F. K. Tittel and J. R. Cavallaro: Generation of nondiffracting Bessel Beams with Fabry-Perot interferometer, *J. Opt. Soc. Am.* A, 14(11), pp.: 3009-3013, (1997)
2. M. Erdelyi, Z. L. Horvath, G. Szabo, Zs. Bor, F. K. Tittel, Joseph R. Cavallaro, Michael C. Smayling: Generation of Diffraction-Free Beams for Applications in Optical Microlithography, *J. Vac. Sci. Technol.* B 15(2) Mar/Apr 287-292 (1997).
3. M. Erdelyi, Z. L. Horvath, Zs. Bor, G. Szabo, J. R. Cavallaro, Michael C. Smayling and F. K. Tittel: Optical microlithography with nearly nondiffracting beams, Optical Microlithography X, Santa Clara, CA (March 9-14, 1997); SPIE Proc. 3051, 959-966, (1997)
4. Miklos Erdelyi, Zs. Bor, William L. Wilson, Michael C. Smayling and Frank K. Tittel: Simulation of Coherent Multiple Imaging by means of Pupil Plane Filtering in Optical Microlithography, (submitted to JOSA A)
5. M. Erdelyi, A. Kroyan, K. Osvay, Zs. Bor, W. L. Wilson, M. C. Smayling and F. K. Tittel: Coherent Multiple Imaging by means of Pupil Plane Filtering, Optical Microlithography XII, Santa Clara, CA (March 17-19, 1999); SPIE Proc. 3679 (1999).
6. H. F. Talbot. Philos. Mag., IX, 401 (1836).
7. B. Rayleigh Philos. Mag. XI, 196-205 (1881).
8. H. Fukuda, T. Terasawa, and S. Okazaki, "Spatial filtering for depth of focus and resolution enhancement in optical lithography," J. Vac. Sci. Technol. B **9(6)**, 3113-3116 (1991).
9. Prolith/2 User's Manual, FINLE Technologies Inc. pp.:B-16 (1996)